

Robust Control of an Islanded DC Microgrid using H_∞ Loop-shaping Design Considering Parametric Uncertainties

Ruchi Sharma

Department of Electrical Engineering
Indian Institute of Technology (BHU)
Varanasi, India
ruchisharma.rs.eee20@itbhu.ac.in

Avirup Maulik

Department of Electrical Engineering
Indian Institute of Technology (BHU)
Varanasi, India
avirupmaulik@gmail.com

Shyam Kamal

Department of Electrical Engineering
Indian Institute of Technology
Varanasi, India
shyamkamal.eee@iitbhu.ac.in

Abstract—A robust decentralized control method is proposed in this paper for an islanded DC microgrid. A state-space model of the islanded DC microgrid system is derived based on the small-signal model of the system. Parametric uncertainties like load resistance, filter inductance and capacitance are modelled using the upper linear fractional transformation technique. A loop-shaping H_∞ controller is designed to ensure robust stability and satisfaction of desired performance criteria. The proposed control technique is applied to an islanded DC microgrid test system comprising a dispatchable distributed generation unit, a photovoltaic unit following the maximum power point tracking algorithm, and a battery energy storage system unit. Simulation studies validate the efficacy of the proposed control approach for an islanded DC microgrid.

Index Terms—DC microgrid, Robust control, Robust stability, H_∞ loop shaping

I. INTRODUCTION

Recently, small-scale generation sources, known as distributed generation (DG), are being added close to the customer site to meet load demands partly or fully. DG can be non-dispatchable (renewable-based sources like photovoltaic (PV) and wind) or dispatchable (controllable sources like microturbine (MT), fuel cell (FC), diesel generator, gas turbine (GT), etc.). A medium voltage (MV) or low voltage (LV) distribution network comprising DG, storage units, and controllable loads in a clearly defined control area is called a microgrid (μG) [1]. AC μG s are more widely used. However, DC-Microgrid ($DC\mu G$)s are also becoming popular for applications like data centres, remote rural electrification, smart buildings, etc., [2].

The control schemes for voltage control of a $DC\mu G$ can be broadly classified as centralized, decentralized, and distributed. Master-slave control is an example of a centralized control scheme, where one DG unit maintains the DC link voltage, while others follow pre-set power references [3]. The Master-slave control is suitable for a small $DC\mu G$. The reliability of operation can be enhanced by adopting a decentralized control architecture. Droop control is an example of a decentralized scheme, where individual DG units receive commands from local controllers. A hierarchical control architecture was proposed in [4], where the primary level involved droop control for communication-less power sharing among multiple dispatchable DG units. The secondary and tertiary controls perform voltage restoration and optimal

operation functions. Several modifications of the basic droop control strategy, like robust droop [5], adaptive droop [6], and optimal droop [7], have been reported. Distributed control schemes incorporate the benefits of centralized and decentralized control philosophies and involve communication between neighbouring units [8], [9]. Robust control techniques have also been used for voltage control of $DC\mu G$ s. A robust decentralized scheme was proposed for voltage control of a $DC\mu G$ incorporating uncertainties of plug and play (PnP), topological changes, and load [10]. A combination of L_2 norm and H_∞ performance criterion was used in the above work. The authors in [11] modelled parametric uncertainties using a “Lebesgue-measurable matrix” and implemented a centralized H_∞ control approach for a $DC\mu G$.

In this work, a decentralized H_∞ loop-shaping design (H_∞ LSD) control scheme is designed for a small isolated $DC\mu G$ system comprising a dispatchable DG source, PV unit, and a battery energy storage system (BESS). The robust controller is designed for all the units. Parametric uncertainties of load and filter elements and disturbances are considered using a structured upper linear fractional transformation (ULFT) representation. The efficacy of the proposed approach is validated using simulation studies.

II. NOMINAL MODEL OF THE $DC\mu G$

The $DC\mu G$ comprises a dispatchable source, a PV unit, and a BESS, as shown in fig. 1. The dispatchable source and the PV units are interfaced with the DC bus using buck converters, while the BESS is interfaced using a bi-directional buck-boost converter.

A. Nominal small-signal Model

The small-signal averaged model of the system is shown in fig. 2. The output capacitances of the three converters are clubbed and represented by a single capacitor C_{eq} in the small-signal model. All upper-case variables denote quiescent operating points, while lower-case variables with hats denote small perturbations of variables around quiescent operating points. For instance, D_1 denotes the quiescent operating duty cycle of the buck converter used with the dispatchable unit, and \hat{d}_1 denotes a small perturbation. The

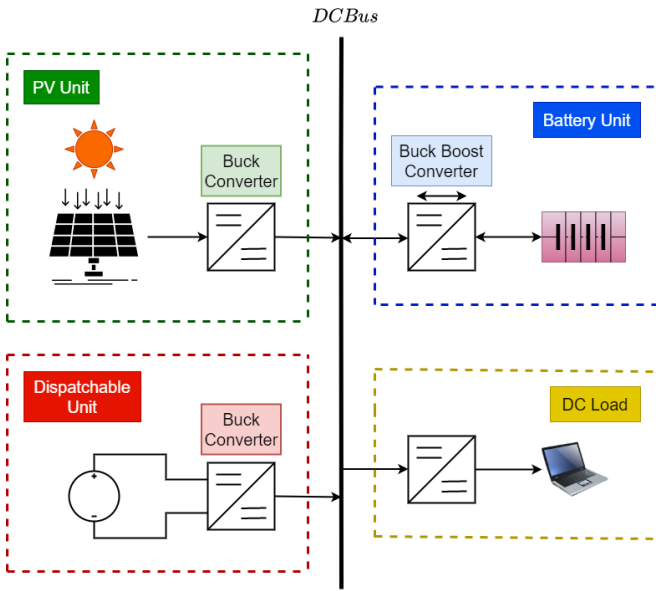


Figure 1. DCμG test System

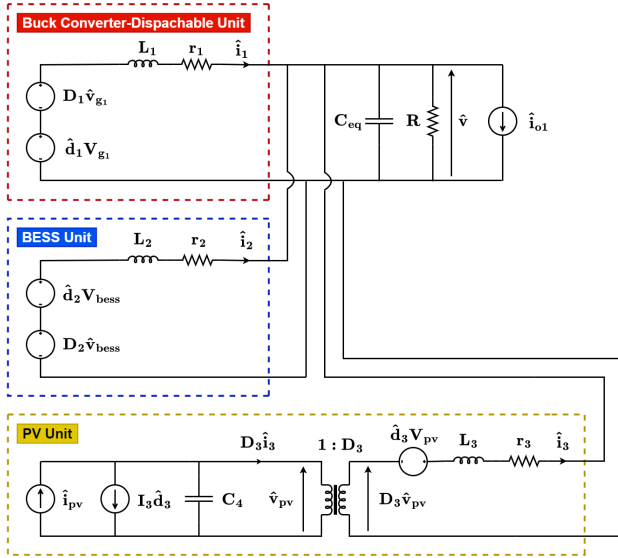


Figure 2. DCμG small-signal model

small-signal linear state space model of the system is as follows:

$$\frac{d\hat{v}}{dt} = -\frac{1}{RC_{eq}}\hat{v} + \frac{1}{C_{eq}}\hat{i}_1 + \frac{1}{C_{eq}}\hat{i}_2 + \frac{1}{C_{eq}}\hat{i}_3 - \frac{1}{C_{eq}}\hat{i}_{o1} \quad (1)$$

$$\frac{d\hat{i}_1}{dt} = \frac{1}{L_1}(-\hat{v} - r_1\hat{i}_1 + \hat{d}_1V_{g1} + D_1\hat{v}_{g1}) \quad (2)$$

$$\frac{d\hat{i}_2}{dt} = \frac{1}{L_2}(-\hat{v} - r_2\hat{i}_2 + \hat{d}_2V_{bess} + D_2\hat{v}_{bess}) \quad (3)$$

$$\frac{d\hat{i}_3}{dt} = \frac{1}{L_3}(-\hat{v} - r_3\hat{i}_3 + \hat{d}_3V_{pv} + D_3\hat{v}_{pv}) \quad (4)$$

$$\frac{d\hat{v}_{pv}}{dt} = \frac{1}{C_4}(-D_3\hat{i}_3 - I_3\hat{d}_3 + \hat{i}_{pv}) \quad (5)$$

In the above state-space representation, the state-variable vector is: $\mathbf{x} = [\hat{v}, \hat{i}_1, \hat{i}_2, \hat{i}_3, \hat{v}_{pv}]^T$, the control input vector

comprises the duty cycles: $\mathbf{u} = [\hat{d}_1, \hat{d}_2, \hat{d}_3]^T$, and the disturbance vector is: $\mathbf{w} = [\hat{i}_{o1}, \hat{v}_{g1}, \hat{v}_{bess}, \hat{i}_{pv}]^T$. We can expand the above state space model to include more generation and storage units. However, the above model does not include parametric uncertainties. Also, the state equations for each unit are coupled with state variables belonging to other units. For example, in eq. (1), terms involving \hat{i}_2 and \hat{i}_3 represent the interaction between the dispatchable unit, the PV and the BESS.

B. Decoupling of interactive states

This work aims to design fully decentralized primary controllers for the units so that local control units use only local measurements. Therefore, in this paper, we have designed individual controllers for each converter using local measurements of the same converter and treating the interaction terms as exogenous disturbance inputs. Therefore, the state space model is modified as follows:

1) *Dispatchable Unit converter*: The state space equation eq. (1) of the dispatchable converter is modified as follows:

$$\frac{d\hat{v}}{dt} = -\frac{G}{C_{eq}}\hat{v} + \frac{1}{C_{eq}}\hat{i}_1 + \frac{1}{C_{eq}}(\hat{w}_{e1}) \quad (6)$$

Where $\hat{w}_{e1} = \hat{i}_2 + \hat{i}_3 - \hat{i}_{o1}$ is the exogenous disturbance input due to interactions with other converters. $G = \frac{1}{R}$. (2) is not modified since no interaction term exists. Therefore, the state space model of the dispatchable unit converter consists of (6) and (2).

2) *BESS converter*: The variation in DC bus voltage (\hat{v}) is the exogenous disturbance input. Therefore, (3) is modified as under:

$$\frac{d\hat{i}_2}{dt} = \frac{1}{L_2}(-r_2\hat{i}_2 + \hat{d}_2V_{bess} + D_2\hat{v}_{bess}) - \frac{1}{L_2}\hat{w}_{e2} \quad (7)$$

Where $\hat{w}_{e2} = \hat{v}$ is the exogenous disturbance.

3) *PV converter*: The variation in DC bus voltage (\hat{v}) is the exogenous disturbance input. Therefore, (4) is modified as under:

$$\frac{d\hat{i}_3}{dt} = \frac{1}{L_3}(-r_3\hat{i}_3 + \hat{d}_3V_{pv} + D_3\hat{v}_{pv}) - \frac{1}{L_3}\hat{w}_{e3} \quad (8)$$

Where $\hat{w}_{e3} = \hat{v}$ is the exogenous disturbance. (5) is not modified since it does not contain interaction terms. Therefore, the state space model of the PV converter is given by (8) and (5). A robust local controller is designed for each converter by treating the interaction terms as exogenous disturbance inputs. The impact of exogenous disturbance inputs (including the interaction terms) on the measured output of each converter is minimized by minimizing the H_∞ norm of the corresponding transfer function. This approach helps mitigate possible instability and poor performance due to interactions between different converters and control loops.

III. H_∞ LOOP-SHAPING DESIGN PROCESS

The first step is to model the parametric uncertainties using the ULFT representation.

A. System model with parametric uncertainty

Parametric uncertainties are modelled for each converter. The equations describing the dynamic behaviour of the uncertain plant (i^{th} converter) are as follows:

$$\begin{aligned}\frac{dx_i}{dt} &= A_i x_i + B_{1i} w_i + B_{2i} u_i \\ z_i &= C_{11i} x_1 + D_{11i} w_i + D_{12i} u_i \\ y_i &= C_{21i} x_1 + D_{21i} w_i + D_{22i} u_i\end{aligned}\quad (9)$$

x_i denotes the states, w_i the disturbance inputs, and u_i the control inputs for the i^{th} converter. z_i and y_i are the controlled and measured outputs, respectively.

1) *Dispatchable unit converter*: The controller of the converter should maintain the DC bus voltage, i.e., track the DC bus voltage reference. In a realistic system, the parameters are not precisely known. However, the parameter values lie within a certain range. The uncertain parameters are modelled as: $G = G_0(1 + p_g \delta_g)$, $L_1 = L_{10}(1 + p_{l1} \delta_{l1})$, $C_{eq} = C_{eq0}(1 + p_{c1} \delta_{c1})$, $r_1 = r_{10}(1 + p_{r1} \delta_{r1})$. G_0 , L_{10} , C_{eq0} , r_{10} represent the nominal values. p_g , p_{l1} , p_{c1} , and p_{r1} denote the per unit variation from the nominal values. $-1 \leq \delta_g, \delta_{l1}, \delta_{c1}, \delta_{r1} \leq 1$. If $p_g = 0.5$, the load conductance can vary up to 50%. For the converter used with the dispatchable unit, states: $x_1 = [\hat{v}, \hat{i}_1]^T$, the disturbance inputs: $w_1 = [\delta_g \hat{v}, \delta_{c1} \frac{d\hat{v}}{dt}, \delta_{l1} \frac{d\hat{i}_1}{dt}, \delta_{r1} \hat{i}_1, \hat{w}_{e1}, \hat{w}_{g1}]^T$, the control input: $u_1 = \hat{d}_1$, the controlled outputs: $z_1 = [\hat{v}, \frac{d\hat{v}}{dt}, \frac{d\hat{i}_1}{dt}, \hat{i}_1]^T$, and the measured output: $y_1 = \hat{v}$. The first four terms in the disturbance input are due to parametric uncertainties. The system matrices are as follows:

$$\begin{aligned}A_1 &= \begin{bmatrix} -\frac{G_0}{C_{eq0}} & \frac{1}{L_{10}} \\ -\frac{1}{L_{10}} & -\frac{r_{10}}{L_{10}} \end{bmatrix}; B_{21} = \begin{bmatrix} 0 \\ \frac{V_{g1}}{L_{10}} \end{bmatrix}; D_{221} = 0 \\ B_{11} &= \begin{bmatrix} -\frac{G_0}{C_{eq0}} & p_g & -p_{c1} & 0 & 0 & -\frac{1}{C_{eq0}} \\ 0 & 0 & -p_{l1} & -\frac{r_{10} p_{r1}}{L_{10}} & 0 & \frac{D_1}{L_{10}} \end{bmatrix} \\ C_{111} &= \begin{bmatrix} 1 & 0 \\ -\frac{G_0}{C_{eq0}} & \frac{1}{L_{10}} \\ -\frac{1}{L_{10}} & -\frac{r_{10}}{L_{10}} \\ 0 & 1 \end{bmatrix}; D_{121} = \begin{bmatrix} 0 \\ 0 \\ \frac{V_{g1}}{L_{10}} \\ 0 \end{bmatrix} \\ D_{111} &= \begin{bmatrix} 0 & 0 & 0 & 0 & 0 & 0 \\ -\frac{G_0}{C_{eq0}} & p_g & -p_{c1} & 0 & 0 & -\frac{1}{C_{eq0}} \\ 0 & 0 & -p_{l1} & -\frac{r_{10} p_{r1}}{L_{10}} & 0 & \frac{D_1}{L_{10}} \\ 0 & 0 & 0 & 0 & 0 & 0 \end{bmatrix} \\ D_{211} &= [0 \ 0 \ 0 \ 0 \ 0 \ 0]; C_{211} = [1 \ 0]\end{aligned}\quad (10)$$

The representation of uncertain parameters as ULFT diagonal Δ block is:

$$\begin{bmatrix} \delta_g \hat{v} \\ \delta_{c1} \frac{d\hat{v}}{dt} \\ \delta_{l1} \frac{d\hat{i}_1}{dt} \\ \delta_{r1} \hat{i}_1 \end{bmatrix} = \begin{bmatrix} \delta_g & 0 & 0 & 0 \\ 0 & \delta_{c1} & 0 & 0 \\ 0 & 0 & \delta_{l1} & 0 \\ 0 & 0 & 0 & \delta_{r1} \end{bmatrix} \begin{bmatrix} \hat{v} \\ \frac{d\hat{v}}{dt} \\ \frac{d\hat{i}_1}{dt} \\ \hat{i}_1 \end{bmatrix}\quad (11)$$

2) *BESS converter*: In this work, the BESS controller should track a current (charging/discharging) reference from the control hierarchy's upper layer. The uncertain parameters are $r_2 = r_{20}(1 + p_{r2} \delta_{r2})$, $L_2 = L_{20}(1 + p_{l2} \delta_{l2})$, with $-1 \leq \delta_{r2}, \delta_{l2} \leq 1$. The state variables: $x_2 = \hat{i}_2$, the disturbance inputs: $w_2 = [\delta_{l2} \frac{d\hat{i}_2}{dt}, \delta_{r2} \hat{i}_2, \hat{w}_{bess}, \hat{w}_{e2}]^T$, the control input: $u_2 = \hat{d}_2$, the controlled outputs: $z_2 = [\frac{d\hat{i}_2}{dt}, \hat{i}_2]^T$, and the measured output: $y_2 = \hat{i}_2$. The first two disturbance inputs are due to parametric uncertainties. The system matrices for boosting operation are as follows:

$$\begin{aligned}A_2 &= \frac{-r_{20}}{L_{20}}; C_{12} = \begin{bmatrix} -\frac{r_{20}}{L_{20}} \\ 1 \end{bmatrix}; B_{22} = \frac{V}{L_{20}}; C_{22} = 1 \\ B_{12} &= \begin{bmatrix} -p_{l2} & -\frac{r_{20} p_{r2}}{L_{20}} & \frac{1}{L_{20}} & -\frac{1-D_2}{L_{20}} \end{bmatrix}; D_{222} = 0 \\ D_{212} &= [0 \ 0 \ 0 \ 0]; D_{122} = \begin{bmatrix} \frac{V}{L_{20}} \\ 0 \end{bmatrix} \\ D_{112} &= \begin{bmatrix} -p_{l2} & -\frac{r_{20} p_{r2}}{L_{20}} & \frac{1}{L_{20}} & -\frac{1-D_2}{L_{20}} \\ 0 & 0 & 0 & 0 \end{bmatrix}\end{aligned}\quad (12)$$

The system matrices for buck operation are as follows:

$$\begin{aligned}A_2 &= \frac{-r_{20}}{L_{20}}; C_{12} = \begin{bmatrix} -\frac{r_{20}}{L_{20}} \\ 1 \end{bmatrix}; B_{22} = \frac{V}{L_{20}}; C_{22} = 1 \\ B_{12} &= \begin{bmatrix} -p_{l2} & -\frac{r_{20} p_{r2}}{L_{20}} & -\frac{1}{L_{20}} & \frac{D_2}{L_{20}} \end{bmatrix}; D_{222} = 0 \\ C_{12} &= \begin{bmatrix} -\frac{r_{20}}{L_{20}} \\ 1 \end{bmatrix}; D_{212} = [0 \ 0 \ 0 \ 0] \\ D_{112} &= \begin{bmatrix} -p_{l2} & -\frac{r_{20} p_{r2}}{L_{20}} & -\frac{1}{L_{20}} & \frac{D_2}{L_{20}} \\ 0 & 0 & 0 & 0 \end{bmatrix} \\ D_{122} &= \begin{bmatrix} \frac{V}{L_{20}} \\ 0 \end{bmatrix}\end{aligned}\quad (13)$$

The uncertain parameters are represented as ULFT diagonal Δ block as follows:

$$\begin{bmatrix} \delta_{l2} \frac{d\hat{i}_2}{dt} \\ \delta_{r2} \hat{i}_2 \end{bmatrix} = \begin{bmatrix} \delta_{l2} & 0 \\ 0 & \delta_{r2} \end{bmatrix} \begin{bmatrix} \frac{d\hat{i}_2}{dt} \\ \hat{i}_2 \end{bmatrix}\quad (14)$$

The proposed theory can be used for voltage control applications also if desired.

3) *PV converter*: The controller of the buck converter used with the PV unit should track the maximum power point tracking (MPPT) voltage (V_{pv}). The parametric uncertainties are modelled as $C_4 = C_{40}(1 + p_{c4} \delta_{c4})$, $L_3 = L_{30}(1 + p_{l3} \delta_{l3})$, $r_3 = r_{30}(1 + p_{r3} \delta_{r3})$, with $-1 \leq \delta_{c4}, \delta_{l3}, \delta_{r3} \leq 1$. The state variables are $x_3 = [\hat{v}_{pv}, \hat{i}_3]^T$, the disturbance inputs $w_3 = [\delta_{c4} \frac{d\hat{v}_{pv}}{dt}, \delta_{l3} \frac{d\hat{i}_3}{dt}, \delta_{r3} \hat{i}_3, \hat{i}_{pv}, \hat{w}_{e3}]^T$. The first three terms in the disturbance input vector are due to parametric uncertainties. The control input is $u_3 = \hat{d}_3$. The controlled output vector is given by $z_3 = [\frac{d\hat{v}_{pv}}{dt}, \frac{d\hat{i}_3}{dt}, \hat{i}_3]^T$, while $y_3 = \hat{v}_{pv}$ is the measured output. The system matrices are as follows:

$$\begin{aligned}A_3 &= \begin{bmatrix} 0 & -\frac{D_3}{L_{30}} \\ \frac{D_3}{L_{30}} & -\frac{r_{30}}{L_{30}} \end{bmatrix}; B_{23} = \begin{bmatrix} -\frac{I_3}{C_{40}} \\ \frac{V_{pv}}{L_{30}} \end{bmatrix}; D_{223} = 0 \\ B_{13} &= \begin{bmatrix} -p_{c4} & 0 & 0 & \frac{1}{C_{40}} & 0 \\ 0 & -p_{l3} & -\frac{r_{30} p_{r3}}{L_{30}} & 0 & -\frac{1}{L_{30}} \end{bmatrix} \\ D_{113} &= \begin{bmatrix} -p_{c4} & 0 & 0 & \frac{1}{C_{40}} & 0 \\ 0 & -p_{l3} & -\frac{r_{30} p_{r3}}{L_{30}} & 0 & -\frac{1}{L_{30}} \\ 0 & 0 & 0 & 0 & 0 \end{bmatrix} \\ C_{13} &= \begin{bmatrix} 0 & -\frac{D_3}{L_{30}} \\ \frac{D_3}{L_{30}} & -\frac{r_{30}}{L_{30}} \\ 0 & 1 \end{bmatrix}; D_{123} = \begin{bmatrix} -\frac{I_3}{C_{40}} \\ \frac{V_{pv}}{L_{30}} \\ 0 \end{bmatrix} \\ C_{23} &= [1 \ 0]; D_{213} = [0 \ 0 \ 0 \ 0 \ 0]\end{aligned}\quad (15)$$

The uncertain parameters are represented as ULFT diagonal Δ block as follows:

$$\begin{bmatrix} \delta_{c4} \frac{d\hat{v}_{pv}}{dt} \\ \delta_{l3} \frac{d\hat{i}_3}{dt} \\ \delta_{r3} \hat{i}_3 \end{bmatrix} = \begin{bmatrix} \delta_{c4} & 0 & 0 \\ 0 & \delta_{l3} & 0 \\ 0 & 0 & \delta_{r3} \end{bmatrix} \begin{bmatrix} \frac{d\hat{v}_{pv}}{dt} \\ \frac{d\hat{i}_3}{dt} \\ \hat{i}_3 \end{bmatrix}\quad (16)$$

B. H_∞ LSD procedure

The closed-loop objectives (as “singular values of weighted transfer function”) are specified in the H_∞ synthesis approach [12]. However, the choice of appropriate weights and closed-loop objectives are involved. Also, the nominal plant and the synthesized controller may have an undesirable pole-zero cancellation. An alternative synthesis approach called the H_∞ LSD procedure combines the classical loop-shaping approach with the H_∞ design and obviates the limitations of H_∞ design. Moreover, the H_∞ LSD method is not iterative and computationally efficient. Let matrices $(\tilde{M}, \tilde{N}) \in H_\infty^+$ be the left coprime factorisation of the nominal plant model G . Let the perturbed plant be $G_\Delta = (\tilde{M} + \Delta_{\tilde{M}})^{-1}(\tilde{N} + \Delta_{\tilde{N}})$. $(\Delta_{\tilde{M}}, \Delta_{\tilde{N}})$ are stable but unknown transfer functions representing the plant uncertainties. The aim is to stabilize the family of perturbed plants as follows [13]:

$$G_\epsilon = \{(\tilde{M} + \Delta_{\tilde{M}})^{-1}(\tilde{N} + \Delta_{\tilde{N}}) : \|[\Delta_{\tilde{M}}, \Delta_{\tilde{N}}]\|_\infty < \epsilon\} \quad (17)$$

Where $\epsilon > 0$ denotes the stability margin. The feedback controller K makes the feedback system $(\Delta_{\tilde{M}}, \Delta_{\tilde{N}}, K, \epsilon)$ robustly stable if and only if (G, K) is internally stable and [13]:

$$\left\| \begin{bmatrix} K(I - GK)^{-1}\tilde{M}^{-1} \\ (I - GK)^{-1}\tilde{M}^{-1} \end{bmatrix} \right\|_\infty \leq \epsilon^{-1} \quad (18)$$

The robust stability of the closed-loop system is maximized by minimizing γ defined as follows:

$$\gamma := \left\| \begin{bmatrix} K \\ I \end{bmatrix} (I - GK)^{-1}\tilde{M}^{-1} \right\|_\infty \quad (19)$$

The lowest possible value γ for all stabilizing controllers K is given by :

$$\gamma_0 = (1 - \left\| [\tilde{N}\tilde{M}] \right\|_H^2)^{-\frac{1}{2}} \quad (20)$$

$\|\cdot\|_H$ is the “Hankel norm”. Let $K = UV^{-1}$ represent all controllers which optimize γ . U and V are stable, and the right coprime factorization of K [13]:

$$\left\| \begin{bmatrix} -\tilde{N}^* \\ \tilde{M}^* \end{bmatrix} + \begin{bmatrix} U \\ V \end{bmatrix} \right\|_\infty = \left\| [\tilde{N} \quad \tilde{M}] \right\|_H \quad (21)$$

The above problem can be solved using the algorithm proposed in [14]. The H_∞ LSD process involves the following steps [13]:

- Design a pre-compensator W_1 and a post-compensator W_2 to modify the singular values of the nominal plant G for achieving the desired loop shape. The shaped system becomes $G_S = W_2GW_1$. G_S should not contain any hidden unstable modes.
- Synthesize a robust feedback controller K_S for robust stability of the normalized left coprime factorization of G_S with a stability margin of ϵ . Frequency responses of $K_SW_2GW_1$ and W_2GW_1 will be similar for $\epsilon \geq 0.2$ [12].
- Combine the H_∞ controller K_S with weighting functions W_1 and W_2 to obtain the feedback controller $K_{fb} = W_1K_SW_2$.

Table I
SYSTEM PARAMETERS

Parameter	Value	Parameter	Value
$r_{10} = r_{20} = r_{30}$	0.2Ω	L_{20}	2 mH
L_{10}	1.8 mH	V_{g1}	100 V
C_{eq0}	9.4 mF	V_{bess} (nominal)	24 V
C_{40}	2.0 mF	f_{sw} (Switching frequency)	10 kHz
L_{30}	1.0 mH	V_{pv} (MPPT voltage)	58 V

IV. SIMULATION STUDIES

The proposed control strategy is validated by simulation studies using an islanded small DC μ G system shown in fig. 1.

A. Test System

The nominal value of the DC bus voltage is 48 volts. Nominal values of system parameters are given in table I. The converter filter parameters are chosen to keep the current and voltage ripples under 5%. A Li-Ion BESS unit, having a nominal voltage of 24 V and a rated capacity of 200 Ah, has been considered. The fully charged voltage of the BESS is 27.9357 V, while the nominal discharge current is 86.9565 A. The Ah capacity is 180.8696 Ah at nominal voltage. The internal resistance of the BESS unit is 0.0012 Ω . The initial state of charge is 50%, and the BESS response time is 1 s. The PV system comprises two parallel strings with two series-connected modules in each string. The maximum power of each module is 213.15 W. There are 60 cells in each module. The open-circuit voltage is 36.3 V, and the short-circuit current is 7.84 A. The voltage and current at the maximum power point for each module are 29 V and 7.35 A, respectively. The temperature coefficient of the open-circuit voltage is $-0.36099\%/^\circ C$ while the temperature coefficient of the short-circuit current is $0.102\%/^\circ C$. All the converters' switching frequency (f_{sw}) is 10 kHz [15].

The quiescent point duty cycle for the buck converter used with the dispatchable unit is $D_1 = 0.48$, and the nominal load conductance $G_0 = \frac{1}{3}\mathcal{U}$. The H_∞ LSD controller for the buck converter used with the dispatchable unit is designed considering 50% parameter variation in G , C_{eq} , L_1 , and r_1 from the nominal values. The quiescent point duty cycle for the bi-directional converter used with the BESS unit is $D_2 = 0.50$ for both charging and discharging operations. The H_∞ LSD controller is designed considering 50% parameter variation in r_2 and L_2 from their nominal values. The quiescent point duty cycle for the converter used with the PV unit is $D_3 = 0.82$ and $I_3 = 17.9268$ A. We have considered 50% parameter variation in r_3 , C_4 , and L_3 from their nominal values while designing the H_∞ LSD controller.

B. Simulation Results

The pre-compensator and the post-compensator for the buck converter used with the dispatchable unit are chosen as $W_1(s) = \frac{9.471s^2 + 8222s + 1.648e06}{s^2 + 1.782e04s}$ and $W_2(s) = 1$ to achieve a phase-margin of 67° and a crossover frequency of 504.80 Hz (see fig. 3). Also, the shaped plant has a high dc gain and good disturbance attenuation characteristics. The stability margin of the designed controller is $\epsilon = 0.5947$, which indicates that the robust feedback controller gives the desired frequency response characteristics. The pre-compensator and the post-compensator for the bi-directional converter used

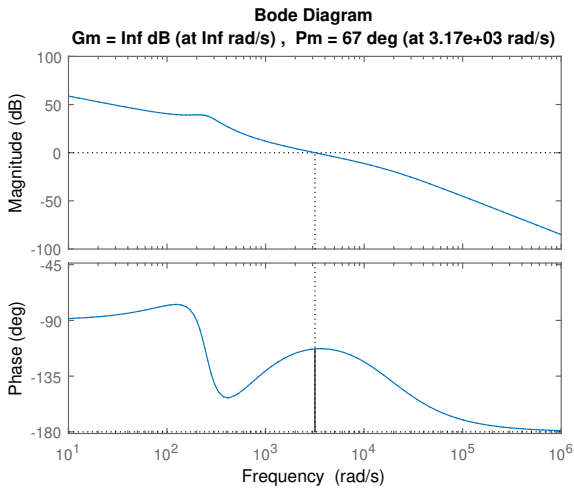


Figure 3. Frequency response of the shaped nominal plant-Buck converter with dispatchable unit

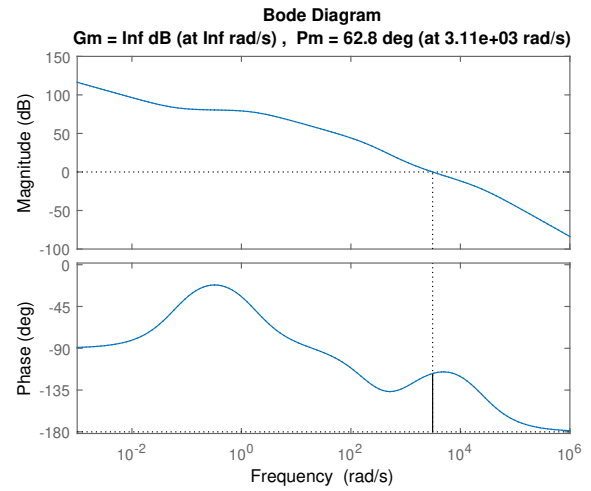


Figure 5. Frequency response of the shaped nominal plant-PV converter

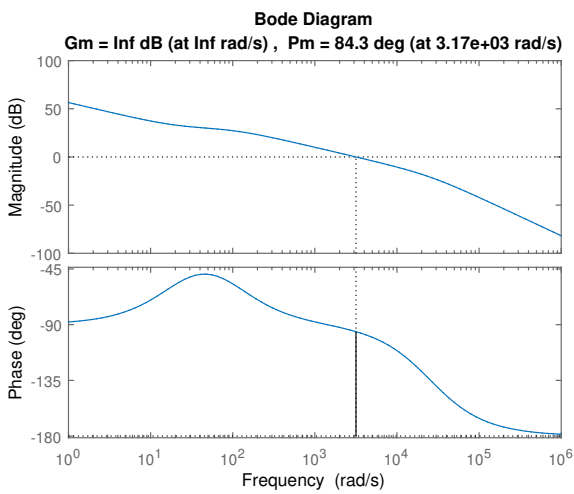


Figure 4. Frequency response of the shaped nominal plant-Bidirectional buck-boost converter

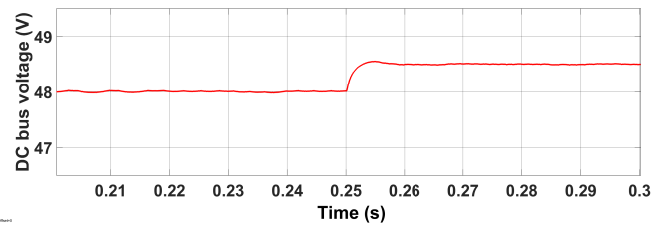


Figure 6. Response with DC bus voltage reference change at $t = 0.25$ s

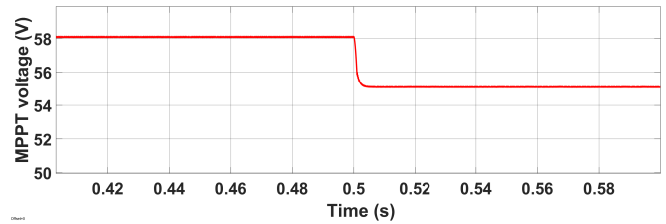


Figure 7. MPPT voltage with reference change at $t = 0.5$ s

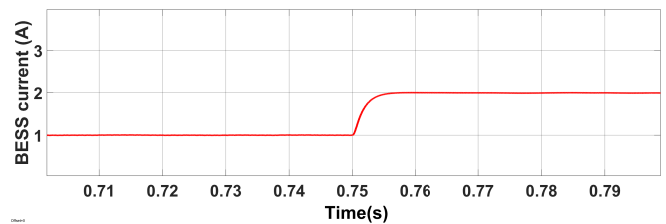


Figure 8. BESS current with reference change at $t = 0.75$ s

with the BESS unit are chosen as $W_1(s) = \frac{0.16s+3.2}{s}$ and $W_2(s) = 1$ for both charging and discharging modes. The plant is shaped to yield a phase margin of 84.35° and a crossover frequency of 504.43 Hz (see fig. 4). The stability margin is $\epsilon = 0.7144$. The pre-compensator and the post-compensator for the converter used with the PV unit are $W_1(s) = \frac{230s+14.38}{s}$ and $W_2(s) = 1$. The shaped plant has a phase margin of 62.81° and a crossover frequency of 495.29 Hz (see fig. 5). The stability margin is $\epsilon = 0.5630$. The controller design is carried out using MATLAB R2015a. The time domain analysis is carried out in SIMULINK.

1) *Tracking performance of nominal closed loop system:*

The following sequence of events is considered:

- $0 \leq t < 0.25$ s: The DC link voltage reference is 48 V, the MPPT voltage reference is 58 V, the BESS discharging current reference is 1 A.
- At $t = 0.25$ s: The DC link voltage reference changes to 48.5 V.
- At $t = 0.50$ s: The MPPT voltage reference changes to 55 V.
- At $t = 0.75$ s: The BESS discharging current reference changes to 2 A.

The DC bus voltage is shown in fig. 6, while the MPPT voltage tracking is shown in fig. 7. The tracking of the BESS current is shown in fig. 8. The time domain results demonstrate proper reference signal tracking with zero steady-state error for all quantities within 0.005 s. Also, the transient response is excellent, with minimal overshoots. Therefore, the designed controller ensures stability and excellent robust performance of the closed-loop system when subjected to reference signal changes.

2) *Robustness to uncertain load, filter parameters, and power injection from PV and BESS units:* The following operating sequence is considered:

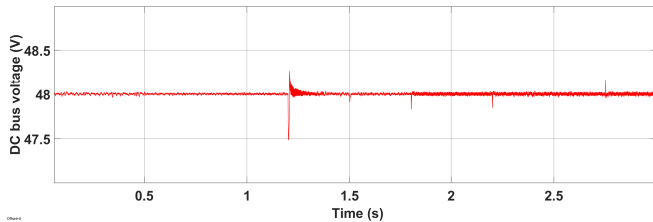


Figure 9. DC bus voltage with load and power injection uncertainty

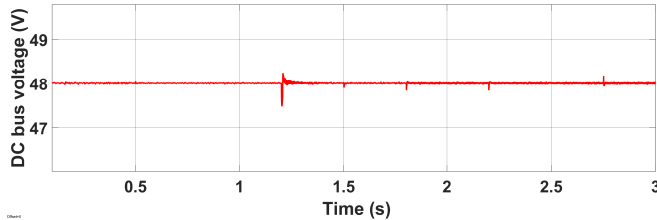


Figure 10. DC bus voltage with filter elements, load and power injection uncertainty

- $0 \leq t < 0.5$ s: The load resistance is 3Ω , the solar irradiation is $500 W/m^2$, and the BESS discharging current reference is 1A.
- At $t = 0.5$ s, the solar irradiation increases to $600 W/m^2$.
- At $t = 0.9$ s, the BESS discharging current reference changes to 2 A.
- At $t = 1.2$ s, the BESS switches to charging mode with a current reference of 2.5 A.
- At $t = 1.5$ s, the solar irradiation reduces to $400 W/m^2$
- At $t = 1.8$ s, the BESS charging current reference becomes 10 A.
- At $t = 2.2$ s, the load resistance becomes 2.25Ω

The plot of the DC link voltage is shown in fig. 9. From fig. 9, it is observed that the DC link voltage stays at 48 V following short and negligible transients after changes in load and power injections from the PV and BESS unit. Therefore, the designed controller is robust and maintains the stability and desired performance of the closed-loop system.

The exact sequence of operation as mentioned above is followed, albeit with $L_1 = 1.9$ mH and $C_{eq} = 9.0$ mF, i.e., with non-nominal filter parameters for the buck converter. The DC bus voltage is shown in fig. 10. In this case, the designed controller exhibits robustness and maintains stability and desired performance of the closed-loop system.

3) *Amenability to PnP operation:* The robust stability and performance of the closed-loop system with the designed controller are validated for PnP operation. The PV unit is switched out at $t = 0.25$ s and again plugged back at $t = 0.35$ s. The DC bus voltage is shown in fig. 11, from which it is observed that the closed-loop system is stable and robust with desired performance under PnP operation with the designed robust controllers.

V. CONCLUSIONS

A robust decentralized controller has been proposed for an islanded DC μ G in this paper. The robust controller has been designed using the H_∞ LSD procedure considering parametric uncertainties of converter filters and loads. The controller for each converter uses local information from the

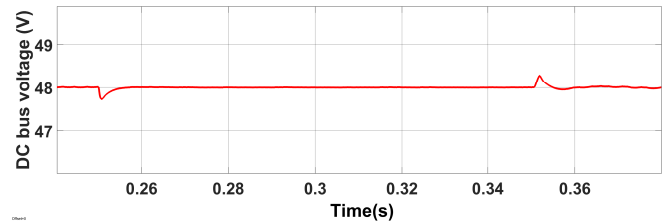


Figure 11. DC bus voltage for PnP operation

converter for which the controller is designed. The interaction terms between different converters have been modelled as exogenous disturbances to avoid possible instability and poor performance. The controller minimizes the impact of exogenous disturbances and parametric uncertainties on the output by minimizing the H_∞ norms. The parametric uncertainties have been modelled using the ULFT structured diagonal Δ matrices. Simulation results on a test DC μ G system reveal that the closed loop system is robust and provides excellent transient performance and zero steady-state error when subjected to parametric uncertainties, load changes, disturbances and PnP operation.

REFERENCES

- [1] R. H. Lasseter and P. Paigi, "Microgrid: A conceptual solution," in *2004 IEEE 35th annual power electronics specialists conference (IEEE Cat. No. 04CH37551)*, vol. 6. IEEE, 2004, pp. 4285–4290.
- [2] F. S. Al-Ismael, "Dc microgrid planning, operation, and control: A comprehensive review," *IEEE Access*, vol. 9, pp. 36 154–36 172, 2021.
- [3] M. Saleh, Y. Esa, and A. Mohamed, "Centralized control for dc microgrid using finite state machine," in *2017 IEEE Power & Energy Society Innovative Smart Grid Technologies Conference (ISGT)*. IEEE, 2017, pp. 1–5.
- [4] J. M. Guerrero, J. C. Vasquez, J. Matas, L. G. De Vicuña, and M. Castilla, "Hierarchical control of droop-controlled ac and dc microgrids—a general approach toward standardization," *IEEE Transactions on industrial electronics*, vol. 58, no. 1, pp. 158–172, 2010.
- [5] Z. Shuai, D. He, J. Fang, Z. J. Shen, C. Tu, and J. Wang, "Robust droop control of dc distribution networks," *IET Renewable Power Generation*, vol. 10, no. 6, pp. 807–814, 2016.
- [6] E. K. Belal, D. M. Yehia, and A. M. Azmy, "Adaptive droop control for balancing soc of distributed batteries in dc microgrids," *IET Generation, Transmission & Distribution*, vol. 13, no. 20, pp. 4667–4676, 2019.
- [7] A. Maulik and D. Das, "Optimal operation of a droop-controlled dcmg with generation and load uncertainties," *IET Generation, Transmission & Distribution*, vol. 12, no. 12, pp. 2905–2917, 2018.
- [8] R. Kumar and M. K. Pathak, "Distributed droop control of dc microgrid for improved voltage regulation and current sharing," *IET Renewable Power Generation*, vol. 14, no. 13, pp. 2499–2506, 2020.
- [9] J. Xiang, Y. Wang, Y. Li, and W. Wei, "Stability and steady-state analysis of distributed cooperative droop controlled dc microgrids," *IET Control Theory & Applications*, vol. 10, no. 18, pp. 2490–2496, 2016.
- [10] M. Shafiq-Rad, M. S. Sadabadi, Q. Shafiq, and M. R. Jahed-Motlagh, "Robust decentralized voltage control for uncertain dc microgrids," *International Journal of Electrical Power & Energy Systems*, vol. 125, p. 106468, 2021.
- [11] M. Mehdi, S. Z. Jamali, M. O. Khan, S. Baloch, and C.-H. Kim, "Robust control of a dc microgrid under parametric uncertainty and disturbances," *Electric Power Systems Research*, vol. 179, p. 106074, 2020.
- [12] D. McFarlane and K. Glover, "A loop-shaping design procedure using h/sub infinity/synthesis," *IEEE transactions on automatic control*, vol. 37, no. 6, pp. 759–769, 1992.
- [13] D.-W. Gu, P. Petkov, and M. M. Konstantinov, *Robust control design with MATLAB®*. Springer Science & Business Media, 2005.
- [14] D. C. McFarlane and K. Glover, *Robust controller design using normalized coprime factor plant descriptions*. Springer, 1990.
- [15] A. Maulik and D. Das, "Stability constrained economic operation of islanded droop-controlled dc microgrids," *IEEE Transactions on Sustainable Energy*, vol. 10, no. 2, pp. 569–578, 2018.